



HAL
open science

The Ig-like domain of Punctin/MADD-4 is the primary determinant for interaction with the ectodomain of neuroligin NLG-1

Semeli Platsaki, Xin Zhou, Bérangère Pinan-Lucarré, Vincent Delauzun, Haijun Tu, Pascal Mansuelle, Patrick Fourquet, Yves Bourne, Jean-Louis Bessereau, Pascale Marchot

► To cite this version:

Semeli Platsaki, Xin Zhou, Bérangère Pinan-Lucarré, Vincent Delauzun, Haijun Tu, et al.. The Ig-like domain of Punctin/MADD-4 is the primary determinant for interaction with the ectodomain of neuroligin NLG-1: Molecular bases of Punctin/MADD-4 interaction with NLG-1. *Journal of Biological Chemistry*, 2020, pp.16267-16279. 10.1074/jbc.RA120.014591 . hal-03021788

HAL Id: hal-03021788

<https://amu.hal.science/hal-03021788>

Submitted on 22 Dec 2020

HAL is a multi-disciplinary open access archive for the deposit and dissemination of scientific research documents, whether they are published or not. The documents may come from teaching and research institutions in France or abroad, or from public or private research centers.

L'archive ouverte pluridisciplinaire **HAL**, est destinée au dépôt et à la diffusion de documents scientifiques de niveau recherche, publiés ou non, émanant des établissements d'enseignement et de recherche français ou étrangers, des laboratoires publics ou privés.



Distributed under a Creative Commons Attribution 4.0 International License

The Ig-like domain of Punctin/MADD-4 is the primary determinant for interaction with the ectodomain of neuroligin NLG-1

Semeli Platsaki¹, Xin Zhou², Bérangère Pinan-Lucarré², Vincent Delauzun¹, Haijun Tu^{2,5}, Pascal Mansuelle³, Patrick Fourquet⁴, Yves Bourne¹, Jean-Louis Bessereau², and Pascale Marchot^{1*}

¹CNRS / Aix-Marseille Univ, Laboratory 'Architecture et Fonction des Macromolécules Biologiques' (AFMB), Marseille - France.

²Univ Lyon / Univ Claude Bernard Lyon 1 / CNRS / INSERM, Institut NeuroMyoGène (INMG), Lyon - France.

³CNRS / Aix-Marseille Univ, Institut de Microbiologie de la Méditerranée (IMM), Plateforme Marseille Protéomique MaP-IBiSA, Marseille – France

⁴Aix-Marseille Univ / INSERM / CNRS, Institut Paoli-Calmettes, Centre de Recherche en Cancérologie de Marseille (CRCM), Marseille Proteomics, Marseille - France

⁵Present address: Institute of Neuroscience, Hunan University, China

*Corresponding author: Lab 'Architecture et Fonction des Macromolécules Biologiques' (AFMB, CNRS/AMU UMR-7257), Faculté des Sciences Campus Luminy - case 932, 163 av. de Luminy, 13288 Marseille CEDEX 09, France. Tel: +33 (0) 491 825 579. Email: pascale.marchot@univ-amu.fr.

Running title: Molecular bases of Punctin/MADD-4 interaction with NLG-1

Keywords: ADAMTS-like, GABA receptor, Punctin/MADD-4, muscle, neuroligin, neuromuscular junction, nicotinic acetylcholine receptor, postsynaptic membrane, protein-protein interaction, synapse.

Abbreviations: ADAMTS(L), A disintegrin and metalloproteinase with thrombospondin type 1 repeats (-like); ECM, extracellular matrix; GABA_AR, GABA type A receptor; HS, heparan sulphate; Ig, immunoglobulin; MDGA, MAM domain-containing GPI-anchored; NLG, neuroligin; NMJ, neuromuscular junction; NRX, neurexin; SEC-MALS, size-exclusion chromatography coupled to multi-angle light scattering; TSP, thrombospondin.

This article contains Supp. Figures S1–S6 and Supp. Experimental Procedures

Punctin/MADD-4, a member of the ADAMTSL extracellular matrix protein family, was identified as an anterograde synaptic organizer in the nematode *Caenorhabditis elegans*. At GABAergic neuromuscular junctions, the short isoform MADD-4B binds the ectodomain of neuroligin NLG-1, itself a postsynaptic organizer of inhibitory synapses. To identify the molecular bases of their partnership, we generated recombinant forms of the two proteins and carried out a comprehensive biochemical and biophysical study of their interaction, complemented by an *in vivo* localisation study. We show that spontaneous proteolysis of MADD-4B first generates a shorter N-MADD-4B form, which comprises four thrombospondin (TSP) and one Ig-like domains and binds NLG-1. A second processing event eliminates the C-terminal Ig-like domain along with the ability of N-MADD-4B to

bind NLG-1. These data identify the Ig-like domain as the primary determinant for N-MADD-4B interaction with NLG-1 *in vitro*. We further demonstrate *in vivo* that this Ig-like domain is essential, albeit not sufficient per se, for efficient recruitment of GABA_A receptors at GABAergic synapses in *C. elegans*. The interaction of N-MADD-4B with NLG-1 is also disrupted by heparin, used as a surrogate for the extracellular matrix component, heparan sulphate, and whose high-affinity binding to the Ig-like domain may proceed from surface charge complementarity, as suggested by homology 3D modelling. These data point to N-MADD-4B processing and cell-surface proteoglycan binding as two possible mechanisms that can regulate the interaction between MADD-4B and NLG-1 at GABAergic synapses.

Synapse formation is fundamental for communication between neurons and their target cells. The life cycle of a synapse involves attraction, recognition and interaction between cells, differentiation of the cell membrane into pre- and postsynaptic terminals, and eventually maturation and elimination (1). Proteins involved in synaptic organization fall into two categories: cell adhesion molecules acting upon contact, and secreted factors acting either locally in the extracellular matrix (ECM) as scaffolding proteins or at longer range distances by diffusion (2). A cardinal pair of cell-adhesion molecules essential for excitatory (glutamatergic and cholinergic) and inhibitory (GABAergic and glycinergic) synapse function involves the membrane-tethered neuroligin (NLG) and alpha- or beta-neurexin (NRX α/β) proteins (3-5), whose ectodomains interact trans-synaptically to bridge the pre- and post-synaptic terminals (3, 6-8). Besides the NRXs, the extracellular interactome of the NLGs also includes secreted partners, such as thrombospondin, whose interaction with NLG accelerates synapse formation (9); hevin, which is secreted by astrocytes and bridges isoforms NLG1B and NRX α 1 at excitatory synapses (10); the MAM domain-containing GPI-anchored (MDGA) proteins, which act as negative regulators of synaptic activity by challenging NRX binding to the NLGs (11). The importance of correct synapse formation for cognition is highlighted by the link between mutations in genes encoding synaptic proteins and the occurrence of neurodegenerative conditions, justifying the emerging concept of 'synaptopathies' (12-13). For instance, mutations in the NLG and/or NRX genes have been consistently detected in individuals with autism spectrum disorder (ASD), and mutations in the NRX genes have been associated with schizophrenia (14). Knockdown of the MDGA2 gene in mice resulted in increased excitatory neurotransmission and ASD-associated behaviour (15), while polymorphism in the MDGA1 gene has been linked to schizophrenia (16-17).

Genetic screens for *C. elegans* mutants with abnormal synaptic organization identified gene *Punctin/madd-4*, whose protein products specify cholinergic versus GABAergic identity of neuromuscular junctions (NMJs) (reviewed in 18). In *C. elegans*, body-wall muscles are innervated by both cholinergic and GABAergic motoneurons that express and secrete distinct Punctin/MADD-4 isoforms (19). The long MADD-4L (isoforms a and c, which differ by the presence/absence of two neighbouring residues) is exclusively present at cholinergic synapses where it recruits ionotropic nicotinic acetylcholine receptors. The short MADD-4B (isoform b), which lacks the N-terminal third of

MADD-4L, is present at both cholinergic and GABAergic synapses. (19). At GABAergic synapses, MADD-4B interacts with the ectodomain of NLG-1, the sole NLG in *C. elegans* (20-21), to cluster GABA type A receptors (GABA_ARs) (19, 22). MADD-4B might also interact with NRX at GABAergic NMJs (23). Surprisingly, in the *MADD-4B* knockout mutant, NLG-1 and GABA_AR are distributed in both the cholinergic and GABAergic synapses, indicating that MADD-4B is essential for retaining NLG-1 at GABAergic synapses, while preventing its incorrect recruitment at cholinergic synapses (19). Altogether, these data imply that specific domains of MADD-4L and MADD-4B instruct the proper recruitment of receptors at cholinergic versus GABAergic synapses. In this light, it was proposed that MADD-4L and MADD-4B undergo intermolecular association, and that this event inactivates the ability of MADD-4L to recruit NLG-1 and prevents incorrect GABA_AR clustering at cholinergic NMJs (19, 22).

Punctin/MADD-4 belongs to the poorly understood ADAMTSL (A Disintegrin and Metalloproteinase with Thrombospondin type 1 repeats - Like) family of secreted multi-domain glycoproteins. Members in the family comprise, from the N- to the C-terminal, a Cys-rich domain, a 'spacer' domain, a varying number of thrombospondin type I repeats (TSPs, elsewhere also referred to as 'TSRs'), and unique combinations of several immunoglobulin (Ig)-like domains with most often one exemplary of protease and lacunin (PLAC) or netrin- or Kunitz-type domains (24, and references therein) (**Fig. 1A**). As such, ADAMTSL proteins resemble, in their domain composition, the C-terminal ancillary part of ADAMTS proteins, yet they are devoid of the N-terminal pro-peptide and catalytic and disintegrin domains and of the protease activity that characterise ADAMTS proteins (24). The importance of ADAMTS(L) proteins is highlighted by their role in binding and remodelling the ECM, an active component in synapse formation. The ECM, which is rich in heparan sulphate (HS) and chondroitin sulphate proteoglycans (25-26), promotes the structural consolidation of formed synapses. Conversely, ECM degradation and remodelling allows synapse plasticity and promotes neurite growth (27, 28-30). ADAMTS(L) proteins actively remodel the ECM by degrading HS and chondroitin sulphate proteoglycans (26, 31), binding fibrillins and participating in microfibril assembly/turnover (24, 32-33) and procollagen processing (34). In schizophrenic individuals, overexpression of chondroitin sulphate proteoglycans leads to abnormal architecture of ECM peri-neuronal nets

(27, 30). ADAMTS(L) dysregulation is linked to ECM-related pathologies including arthritis (31), melanoma growth (35), bronchial epithelial dysplasia (36) among others. Interestingly, gene *ADAMTSL3*, one of the two human *madd-4* homologs, is expressed in the central nervous system and was identified as a susceptibility gene for schizophrenia (27).

MADD-4 is the first member of the ADAMTSL family to be identified as a synaptic regulator (19). To better understand the function of MADD-4B at GABAergic synapses, we generated recombinant forms of MADD-4B and of the ectodomain of NLG-1 and carried out a comprehensive biochemical and biophysical analysis of their interaction, buttressed by a complementary *in vivo* analysis. We show that MADD-4B inevitable proteolysis at a well defined site first generates a shorter entity encompassing the N-terminal four TSP and sole Ig-like C2-type domains (herein referred to as ‘N-MADD-4B’), while further processing eliminates the Ig-like domain to generate an even shorter entity comprising the TSP domains only. Quantitative characterisation of the interaction of N-MADD-4B and of its maturation products with NLG-1 points to the Ig-like domain as the primary determinant responsible for NLG-1 binding *in vitro* and for efficient GABA_AR recruitment at GABAergic synapses *in vivo*. Distinct relative affinities of these proteins for heparin, used as a surrogate for heparan sulphate, suggest a role of cell-surface proteoglycans as regulators of the N-MADD-4B interaction with NLG-1. We propose that N-MADD-4B maturation, resulting in elimination of the Ig-like domain, is a plausible regulation mechanism at *C. elegans* GABAergic synapses.

Results and discussion

The ADAMTSL protein MADD-4B comprises, from the N- to the C-terminal, four TSP domains, one Ig-like C2-type module, three additional TSP domains and a PLAC domain (**Fig. 1A**). Initial analysis of a recombinant form of MADD-4B secreted from mammalian (HEK) cells revealed critical cleavage of most of the protein population in two pieces during the earliest steps of production. Western blot tracking of the C-terminal Fc-tag coupled with N-terminal sequencing of the pieces lead to locate the cleavage site upstream to sequence VQVSKED in the linker region that follows the Ig-like domain (data not shown). Since previous analysis of MADD-4B as a guidance cue *in vivo* demonstrated that the C-terminal TSP5-7 and PLAC domains were dispensable for protein functionality (37), we generated a new construct comprising only

the TSP1-4 and Ig-like domains, herein referred to as ‘N-MADD-4B’ (**Fig. 1A**). N-MADD-4B contains a CXX(S/T)CXXG consensus motif for O-fucosylation (38, 39) at the beginning of each TSP domain, along with a NX(T/S) consensus motif for N-glycosylation at Asn362 in the Ig-like domain (**Fig. 1B**). Structural models of the TSP1-4 and Ig-like domains point to an elongated, flexible TSP1-4 domain arrangement, connected to the globular Ig-like domain by an equally flexible hinge (**Fig. 1B, C**). The net positive charge of N-MADD-4B (theoretical pI: 8.8) is reflected in the even distribution of electropositive potentials at the surface of the molecule, apart from the presence of two pockets, respectively more electropositive than the overall surface and highly electronegative, on opposite faces of the Ig domain (**Fig. 1C**).

N-MADD-4B processing in vitro eliminates the Ig-like domain

N-MADD-4B was produced, purified and analysed using standard procedures (see Experimental procedures) (**Fig. 2**). Electrophoretic analysis of the affinity-purified protein revealed a major entity migrating slightly above the 45 kDa marker, along with two to three smaller entities migrating at ca. 35 kDa, 25 kDa and 15 kDa, respectively (**Figs. 2A and 3A**). Peptide mass fingerprinting analysis confirmed that all three entities belonged to N-MADD-4B, albeit with distinct levels of C-terminal coverage (**Supp. Fig. S1**). Intact N-MADD-4B and the 35 kDa entity (45.781 kDa and 31.345 kDa, respectively, by MALDI-TOF-TOF mass spectrometry (MS), **Supp. Fig. S2**) could be separated from each other by cation exchange (**Fig. 2B**) but not size-exclusion chromatography (**Fig. 2C**). Consistently, analytical size-exclusion chromatography coupled to multi-angle light scattering (SEC-MALS) pointed to two overlapping peaks of 45.7 kDa and 33.7 kDa, respectively (**Supp. Fig. S3**). The ca. 2.9 kDa difference between the theoretical mass of the naked N-MADD-4B polypeptide (42.9 kDa) and the experimental values obtained by electrophoresis, MS and SEC-MALS, may reflect, e.g., presence of a N-glycan linked to Asn362 and/or O-glycans at consensus motifs (see **Fig. 1**). Over time, the purified 35 kDa entity further led to a ca. 25 kDa piece (**Fig. 3A**). Thorough analysis of the fragmentation process pointed to a time- and temperature-dependent process not prevented by protease inhibitors (**Supp. Fig. S4**).

To identify the cleavage sites in N-MADD-4B, samples of intact and processed N-MADD-4B were subjected to N-terminal sequencing (**Fig. 3A, Table 1**). The most abundant sequence detected (ca. 90%)

corresponded to the N-MADD-4B N-terminus (**Fig. 3B**). Minor abundance sequences ($\leq 10\%$) indicated cleavage between the TSP1 and TSP2 domains (S⁷⁸-R⁸⁷), within the TSP3 domain (sequence T¹⁷⁵-L¹⁸⁴) and between the TSP4 and Ig-like domains (S²⁷³-E²⁸², R²⁷⁵-K²⁸⁴ and E²⁸²-G²⁹¹). The entity cleaved between TSP1 and TSP2 corresponds to the most abundant fragment of ca. 25 kDa (**Fig. 3A, lane 2**). A similar fragment was generated upon spontaneous processing of a recombinant 'TSP1-4' protein (see below, and **Supp Fig. S4**). In the absence of further processing, cleavage before the T¹⁷⁵-L¹⁸⁴ sequence would generate N- and C-terminal moieties of ca. 19 kDa and 23 kDa, respectively, while cleavage before or within the S²⁷³-E²⁸² sequence would generate N- and C-terminal moieties of ca. 31 kDa and 10 kDa, respectively. The two N-terminal moieties were occasionally detected by electrophoresis (Figs. 2A, 3A, 4A), while the C-terminal moieties were detected neither by N-terminal sequencing nor by electrophoresis. These data suggest that N-MADD-4B processing readily eliminates the C-terminal Ig-like domain to generate a 'N-MADD-4B_{ΔIg}' moiety comprising only the TSP1-4 domains.

Inability to prevent N-MADD-4B processing using protease inhibitors led us to suspect a maturation mechanism distinct from accidental proteolysis. Spontaneous cleavage at physiological pH was first reported for cytochrome c (40) and rabbit muscle aldolase (41) and proposed to act as a 'molecular clock', i.e., a natural mechanism regulating protein activity (42). Spontaneous cleavage occurs often, but not exclusively, at Asn/Asp-Gly dipeptide sites, through non-enzymatic deamidation of Asn or dehydration of Asp, leading to intermediates prone to further hydrolysis (43). The ability of a protein to undergo a deamidation reaction depends on the conformation and/or solvent exposure of the Asn-Gly doublet (42-43). The Ig-like domain of N-MADD-4B contains two such dipeptides (N³²¹G, N³³⁶G), likely located in surface loop regions (**Fig. 1B**). However, Ala substitution of these two Asn residues did not prevent the loss of the Ig-like domain (**Supp. Fig. S5**). Asn/Asp-X dipeptides comprising a second residue other than Gly (Ala>Ser>Leu>Val>Ile in order of reactivity) can also undergo degradation (43). Such doublets are present throughout the N-MADD-4B sequence (D⁷⁴S, D¹²⁴A, D¹⁷⁶G, N²⁰¹V, D²²²S, D²⁵⁰A, N²⁸⁰A), of which D⁷⁴S and D¹⁷⁶G are near or within low abundance N-terminal sequences (S⁷⁸-R⁸⁷ and T¹⁷⁵-L¹⁸⁴, respectively) (**Fig. 3, Table 1**). The implication of deamidation in physiological responses *in vivo*, including signal transduction during DNA-damage induced cell apoptosis (44) and in the enhanced cell-adhesion properties of ECM proteins (45), supports

the concept of deamidation regulating protein functionality. Whether this is the case for MADD-4B *in vivo* would be worth investigating.

The Ig-like domain of N-MADD-4B is essential for the interaction with NLG-1 *in vitro*

The ability of N-MADD-4B and N-MADD-4B_{ΔIg} to interact with the ectodomain of NLG-1 was assayed using microscale thermophoresis (MST), along with data fitting to binding equations considering either the law of mass action (calculation of the equilibrium dissociation constant, Kd) or the Hill model (calculation of the half maximal effective concentration, EC₅₀) (**Fig. 4, Table 2**). Direct binding of N-MADD-4B to labelled NLG-1 occurred with comparable Kd or EC50 values in the 0.5 μM range, while N-MADD-4B_{ΔIg} generated no binding signal (**Fig. 4A**), suggesting that the Ig-like domain is the primary determinant for N-MADD-4B interaction with NLG-1. Full competition between labelled and unlabelled NLG-1 for binding to N-MADD-4B led to Kd and EC50 values again comparable to each other, and less than 3-fold higher than those obtained for direct binding (i.e., corresponding to only minimal differences in free energy requirements for binding), thereby confirming the binding specificity (**Fig. 4B**). If the Hill coefficient is fixed at the value of 1 (for a 1:1 binding stoichiometry), the Hill model reverts to the Kd model. However, except for binding reactions of higher order stoichiometry, the Hill model may also apply to binding events involving multiple steps (46). Here, the multi-domain organization of N-MADD-4B may trigger primary and secondary binding events accounting for the slightly better statistics obtained upon data fitting to the Hill model.

Finally, to preclude possible bias associated with the use of processed proteins, we generated recombinant forms of the TSP1-4 and Ig-like domains and explored their respective interaction with NLG-1. NLG-1 was found to bind the labelled Ig-like domain with Kd/EC50 values in the 6 μM range (**Fig. 4C, Table 2**), i.e., an affinity lower, by one order of magnitude, than that for the intact N-MADD-4B, while no binding of TSP1-4 to labelled NLG-1 was observed (**Fig. 4D**). These data confirm the primary requirement of the Ig-like domain for N-MADD-4B interaction with NLG-1, and support secondary involvement of at least one of the TSP1-4 modules, recruited upon binding proximity when tethered to the Ig-like domain through the flexible intervening linker (see **Fig. 1**), albeit not able to bind NLG-1 by its/their own.

MADD-4 was shown to be essential in muscle arm guidance during the process of NMJ formation in *C. elegans*, where it acts as a molecular cue, while initial analysis of MADD-4B suggested that its TSP1 and Ig-like domains are both crucial for protein functionality (37). It was also suggested that the Ig-like domain alone is sufficient for MADD-4B interaction with NRX, while domains TSP3-4 may contribute some degree of synergy (23). Consistent with these reports is the radical effect of the loss of the Ig-like domain on N-MADD-4B interaction with NLG-1 *in vitro*. In addition, the reduced affinity of the isolated Ig-like domain for NLG-1, relative to that of N-MADD-4B, suggests that one or more of the TSP1-4 domains may reinforce the primary binding of the Ig-like domain. Intramolecular synergy has been reported previously within the ADAMTS proteins, where the catalytic domain alone is often not fully active and needs the disintegrin domain for substrate binding, while the ancillary domains define substrate specificity (47-48). In turn, NLG complexes with demonstrated or proposed synergistic ligand binding are exemplified by those formed by mammalian NLGs with MDGA or NRX α , respectively. Indeed, distinct Ig-like domains of MDGA were shown to bind distinct sites at the surface of the NLG dimer, thereby clamping the two subunits together (11, 49-50). Differently, overlaying the LNS6 domain in the L-shaped, long NRX α molecule with that forming the short NRX β molecule as bound to NLG pointed to the LNS3 and/or LNS4 domains in NRX α as possible secondary binders reinforcing, on the same NLG subunit, the primary interaction of domain LNS6 common to the two NRX forms (51-52).

Heparin interacts with NLG-1, N-MADD-4B and TSP1-4 with distinct relative affinities

Proteoglycans are active components of the ECM. The negatively charged HS chains of HS proteoglycans regulate the interactions between synaptic components, such as the mammalian NRX proteins and their NLG or Leucine-Rich Repeat TransMembrane (LRRTM) partners (53). To explore the potential effect of HS on the N-MADD-4B interaction with NLG-1, we used heparin as a surrogate for HS, along with complementary MST and affinity chromatography approaches (**Fig. 5, Table 3**). Upon direct binding in the presence of 250 μ M heparin, the affinity of intact N-MADD-4B for labelled NLG-1 was found to be reduced by ca. 4-fold, indicating heparin binding to either N-MADD-4B or NLG-1, or both (**Fig. 5A**). Full competition between heparin binding and formation of the N-MADD-4B/labelled NLG-1 complex, with an EC50 value intermediate to those determined for formation of the N-MADD-4B/labelled NLG-1 complex in

absence/presence of heparin, confirmed heparin-driven destabilisation of the N-MADD-4B interaction with NLG-1 (**Fig. 5B**). To preclude possible bias from molecular heterogeneity of commercial heparin, we repeated this experiment using highly purified samples of decameric heparin and HS: the same results were obtained (data not shown).

The relative affinities of N-MADD-4B (processed sample containing both the intact protein and N-MADD-4B Δ Ig moiety), TSP14 and NLG-1 for heparin were assessed by affinity chromatography with conductivity recording and by SDS-PAGE (**Fig. 5C**). All proteins were retained on immobilised heparin, yet elution of N-MADD-4B required a ca. 3-fold higher ionic strength (900 mM NaCl, 81.9 mS/cm) than elution of N-MADD-4B Δ Ig, TSP1-4 or NLG-1 (elution at ca. 22 mS/cm, i.e., 340 mM NaCl). A similar analysis of the interaction of two variants of the Hedgehog morphogen (a key mediator of embryonic development) with immobilised heparin correlated elution at 37 mS/cm and 52 mS/cm conductivity with Kd values of 6.8 μ M and 0.8 μ M, respectively, as measured by surface plasmon resonance (54). Linear extrapolation from these two sets of data led to estimated Kd values of ca. 11 nM and 58 μ M for heparin binding by N-MADD-4B and by the other three proteins, respectively. To confirm the significant (10^4 -fold) difference in estimated affinities, we also loaded the recombinant Ig-like domain onto the same heparin column, albeit using a high salt starting buffer to compensate its lower solubility (**Fig. 5D**). Not only did the Ig-like domain fully bind to heparin, despite its loading at an ionic strength higher than those leading to N-MADD-4B Δ Ig, TSP1-4 and NLG-1 elution from the column, but also its elution required as high a ionic strength as did elution of intact N-MADD-4B. Hence, heparin-driven destabilisation of the N-MADD-4B interaction with NLG-1 proceeds from specific, high affinity binding of heparin to the Ig-like domain of N-MADD-4B.

ADAMTS proteins were shown to degrade the protein core of sulphated proteoglycans such as aggrecan and versican (25-26). The critical contribution of the negatively charged sulphated glycan chains to this phenomenon suggested a primarily electrostatic interaction (48). While the ADAMTSL proteins are devoid of the catalytic domain and activity found in their ADAMTS relatives, they share some of the ADAMTS ancillary domains (TSP, Ig, PLAC) (**Fig. 1A**). Our structural model of the Ig-like domain evidences a highly electropositive surface pocket (**Fig. 1C**) of a suitable

size for lodging heparin with high affinity. *In vivo*, HS or chondroitin sulphate proteoglycans are thought to generate signalling gradients guiding protein interactions and/or secreted protein release, as is the case for the HS-dependent interaction between the secreted glycoprotein, Wnt, and its partner, Frizzled (55). Binding of ADAMTS4/5 to syndecan has been proposed to trigger signalling events through activation of the MAP kinase pathway (28). Whether, and how, HS proteoglycans regulate the N-MADD-4B interaction with NLG-1 in *C. elegans* remains to be investigated.

The Ig-like domain of N-MADD-4B is necessary but not sufficient for rescuing GABA_AR clustering in *C. elegans madd-4* mutants

To investigate *in vivo* the functional relevance of the interaction between the Ig-like domain and NLG-1 observed *in vitro*, we expressed GFP-fused N-MADD-4B or TSP1-4 in *madd-4* null mutants expressing RFP-tagged GABA_AR from the CRISPR/Cas9-engineered locus *unc-49::rfp(kr296)* (Fig. 6A, B'). Compared to wild-type animals, in *madd-4* null mutants, synaptic expression of GABA_AR was found to be reduced by 50% (Fig. 6A, C). Expression of N-MADD-4B-GFP in GABAergic neurons rescued GABA_AR expression to wild-type levels (Fig. 6B, C). Moreover, N-MADD-4B-GFP was found to colocalize with UNC-49, a feature further supporting the hypothesis that N-MADD-4B alone can promote GABA_AR clustering. In contrast, expression of TSP1-4-GFP did not rescue GABA_AR expression nor promoted GABA_AR clustering (Fig. 6B, C). These data point to a critical role of the Ig-like domain for MADD-4 function at GABAergic synapses *in vivo*.

To further explore the role of this domain *in vivo*, we expressed a GFP-fused Ig-like domain in the *madd-4* null mutants and assessed its ability to rescue the *madd-4* null phenotype (Supp. Fig. S6). The Ig-GFP fusion protein did not sharply localize to GABAergic synapses, but instead, made enlarged punctae in the nerve cord region. Moreover, the Ig-GFP fusion protein did not rescue GABA_AR expression defects, indicating that the Ig-like domain alone is not sufficient for GABA_AR recruitment. Hence, *in vivo*, synergistic interaction of the Ig-like domain and one or more TSP domains with NLG-1 is likely required for ensuring N-MADD-4B synaptic function.

Our results, in demonstrating the essential role of the Ig-like domain of MADD-4B for NLG-1 binding *in vitro* and *in vivo*, raise the question of whether the shedding of the Ig-like domain could be a yet undescribed mechanism for regulation of GABA_AR

recruitment at GABAergic synapses. Autocatalytic processing of the ADAMTS2 or ADAMTS4 C-terminus has been reported to generate cleavage products thought to regulate catalytic activity (34, 56). Similarity of ADAMTSL proteins to the ancillary domains of ADAMTS suggested that these domains may act as regulators of ADAMTS activity (57). Papillin, an ADAMTSL relative, was shown to act *in vitro* as a non-competitive inhibitor of ADAMTS2 (58). At the *C. elegans* NMJ, MADD-4B processing could either be controlled by a matrix metalloprotease (potentially an ADAMTS family member) or be an auto-processing event. Taking a step back, one may wonder whether the MADD-4B primary cleavage event identified from the conditioned culture medium reflects a regulatory mechanism *in vivo*, aimed at generating not only N-MADD-4B as described herein, but also a complementary 'C-MADD-4B' moiety, comprising the three TSP and one PLAC domains C-terminal to MADD-4 (Fig. 1A). While N-MADD-4B acts at the inhibitory, GABAergic synapse, C-MADD-4B could migrate to excitatory, cholinergic NMJs, where its interaction with MADD-4L would prevent improper GABA_AR recruitment, as previously proposed for intact MADD-4B (19). Whether the C-MADD-4B moiety could prevent the Ig-like domain from interacting with NLG-1 in the MADD-4L context remains to be assayed. Finally, from an evolutionary perspective it must be pointed out that the Ig-like domain in MADD-4 resembles more, in length and sequence, the first of the three Ig-like domains in human ADAMTSL3 (36% identity, versus 23 and 26% for the other two domains - BLASTn search, data not shown) (Fig. 1A). It would be worth investigating whether this domain plays a central role for ADAMTSL3 function, as does the Ig-like domain for MADD-4B function.

Conclusions

Previous studies identified the short MADD-4B isoform as a key molecule for the organization of GABAergic synapses (18). How MADD-4B activity is regulated remains, however, elusive. The current study evidences a critical role of the Ig-like domain contained in the central part of MADD-4B, both for *in vitro* binding to NLG-1 and for *in vivo* clustering of GABA_AR, and points to two novel regulatory mechanisms of MADD-4B activity. First, we show that the Ig-like domain is the primary determinant for N-MADD-4B binding to heparin, whose competition with NLG-1 binding suggests a regulatory role by cell-surface proteoglycans at the synapse. Second, we identified an unexpected self-maturation process of N-MADD-4B *in vitro*, which sheds the Ig-like domain. An increasing number of studies report the shedding of synaptic protein

domains by various domains *in vivo*. Whether self-processing is also used *in vivo* to regulate the activity of synaptic determinants is an appealing hypothesis.

Experimental procedures

Production of recombinant proteins

The *C. elegans* genes and construct boundaries used for recombinant protein production are as follows: (i) the ectodomain of NLG-1 (residues Tyr18-Glu607; Uniprot C40C9.5); (ii) a truncated version of MADD-4B encompassing the TSP1-4 repeats and subsequent Ig-like C2-type domain ('N-MADD-4B') (residues Asp369-Ser743 of MADD-4 isoform a, Uniprot F53B6.2); (iii) the TSP1-4 repeats of N-MADD-4B ('TSP1-4') (residues Asp369-Phe645 of MADD-4 isoform a); (iv) the Ig-like C2-type domain of N-MADD-4B ('Ig-like') (residues Glu646-Ser743 of MADD-4 isoform a).

The NLG-1, N-MADD-4B and TSP1-4 encoding sequences were N-terminally fused to sequences for a signal peptide ensuring protein secretion from mammalian cells (secreted human placental alkaline phosphatase peptide for NLG-1; mouse IgK peptide for N-MADD-4B and TSP1-4), C-terminally prolonged by sequences encoding a 3C-Protease cleavage site and a human Fc domain, and inserted into a pYD7 vector (National Research Council Canada, Biotechnology Research Institute) using In-Fusion cloning (Takara-Bio). The constructs were transfected into adherent HEK293-EBNA cells (59) using polyethylenimine (Polysciences) and stable cell lines were generated using blasticidine (20-50 µg/ml) for selection pressure. The proteins were routinely produced from 500 ml of stable cell lines cultured at 37°C in Dulbecco's Modified Eagle Medium (DMEM) supplemented with foetal bovine serum (FBS) 10% (v/v) and blasticidine 5 µg/ml. Proteins were then expressed over 5-8 days in DMEM supplemented with FBS 2% (v/v) and valproic acid 1.25 mM, at 37°C for NLG-1 and at 30°C for N-MADD-4B and TSP1-4.

The Ig-like encoding sequence was N-terminally fused to sequences for a 6xHis tag followed by a thrombin cleavage site, and cloned into a pET28a vector (Twist Bioscience) suitable for bacterial expression. The construct was transformed into *Escherichia coli* (BL21_DE3) and cells were grown at 37°C. Protein expression was induced at OD₆₀₀ 0.2-0.6 using IPTG 0.5 mM and allowed to proceed overnight at 17°C.

Protein purification

All liquid chromatography was performed at room temperature using an ÄKTA Purifier apparatus (GE Healthcare). Maintaining protease inhibitors throughout all purification steps was not manageable, while their presence was reported not to prevent proteolysis of ADAMTSL proteins (32). Instead, we tested their impact on the kinetics of proteolysis of purified intact N-MADD-4B at three temperatures (see below). Conditioned culture medium (500 ml) containing the secreted, Fc-fused NLG-1, N-MADD-4B or TSP1-4 protein was harvested, dialysed against sodium phosphate 100 mM, pH 7.4, NaCl 200 mM (8L, 4°C, overnight), then loaded on a Protein-A affinity column (5 ml; GE Healthcare). The Fc fragment was removed by in-column digestion by GST-tagged 3C-Protease (800 µl at 0.5 mg/ml, overnight, 4°C), and the protein of interest was eluted from the Protein-A column through a GSTrap column (1 ml, GE Healthcare) in the same buffer. For N-MADD-4B only, the fractions eluted from the Protein-A/GST-Trap columns were diluted 10-fold in Hepes 20 mM, pH 7.5, loaded on a MonoS column (1 ml, GE Healthcare) and eluted using a linear gradient of NaCl (0 to 1 M over 20 ml). For all three proteins, the fractions of interest were concentrated by ultrafiltration (10 kDa cut-off membrane, Amicon, Merck-Millipore) and further purified by size-exclusion chromatography on Superdex-200 (16/60 column) or Superdex-75 (10/300 column) in Hepes 20 mM, pH 7.5, NaCl 200 mM.

Bacterial pellets containing the Ig-like domain were resuspended in Hepes 20 mM, pH 7.5, NaCl 500 mM (buffer A), supplemented with DTT 1 mM, DNase 10 µg/ml, MgCl₂ 2 mM and a cocktail of protease inhibitors (Roche). The soluble fraction of the lysate was loaded on Ni Sepharose 6 Fast Flow resin (5 ml in batch, GE Healthcare), which was then washed with buffer A supplemented with NaCl up to 1 M and imidazole 30 mM. The protein was eluted in buffer A supplemented with DTT 1 mM and imidazole 300 mM, and dialysed against buffer A (4°C, overnight). Finally, the protein was concentrated (3 kDa cut-off membrane, Amicon, Merck-Millipore), and further purified by size-exclusion chromatography on Superdex-75 (10/300 column) in the dialysis buffer.

Proteins were analysed by SDS-PAGE under denaturing and reducing conditions (loading buffer containing SDS 4% (w/v) and DTT 500 mM) using 15% (NLG-1, N-MADD-4B, TSP1-4) or 18% gels (Ig-like) stained with Instant Blue (Expedeon). In all cases, protein identity and intact mass were verified by MS procedures (see below). Purified proteins were quantified by absorbance on a NanoDrop

(Thermo Scientific) or UV-vis spectrophotometer (Carry Eclipse), using the theoretical molar extinction coefficients, ϵ at 280 nm, calculated using the ProtParam tool in ExPasy (NLG-1: 82.65 mM⁻¹ cm⁻¹; N-MADD-4B: 67.06 mM⁻¹ cm⁻¹; TSP1-4: 55.47 mM⁻¹ cm⁻¹; Ig-like: 12.55 mM⁻¹ cm⁻¹). They were stored at 4°C or -20°C. For the time-course analysis of N-MADD-4B processing, the protein (ca. 0.4 mg/ml) was maintained at -20°C, 4°C or room temperature in the absence or presence of an EDTA-free protease inhibitor cocktail (Roche) supplemented with EDTA 2 mM, according to the manufacturer's instructions. Aliquots were removed at selected time points, denatured and reduced as above described, and stored at 4°C until SDS-PAGE analysis.

Heparin-affinity chromatography

Chromatography was performed using an ÄKTA Purifier apparatus equipped with an on-line conductimeter. Stock NLG-1, N-MADD-4B and TSP1-4 proteins, diluted to 0.8 mg/ml in Hepes 20 mM, pH 7.5, to lower the NaCl concentration to less than 50 mM, were loaded on a heparin column (5ml, GE Healthcare) pre-equilibrated in and then washed with the same buffer, and eluted using a linear gradient of NaCl (0 to 1.0 M over 40 ml). Stock Ig-like protein (0.8 mg/ml) in buffer A (see above) was loaded on the column, pre-equilibrated in and then washed with the same buffer, and eluted with a linear gradient of NaCl (500 mM to 1.0 M over 45 ml). Fractions of interest were analysed by SDS-PAGE (see above).

Size-exclusion chromatography coupled to multi-angle light scattering (SEC-MALS)

The SEC-MALS-RI-UV setup consisted of an Ultimate3000 HPLC apparatus (including quaternary pump, autosampler, and UV-VIS variable wavelength (diode array) detector) (Thermo Scientific) in line with a DAWN8 multi-angle laser light scattering detector calibrated with titrated BSA, and an Optilab relative refractive interferometer (Wyatt Technology, Santa Barbara, CA). Chromatography was performed at 20°C on Superdex-200 (10/300 column, GE Healthcare) using Hepes 20 mM, pH 7.5, NaCl 200 mM, a flow rate of 0.6 ml/min, and 30 μ l of protein at 2 mg/ml. UV absorbance of the eluents was recorded at 280 nm. The Agilent software was used to control the HPLC, and the Wyatt Astra V software was used for data collection and analysis. Peak alignment and band broadening correction between the UV, MALS, and RI detectors were performed using Astra software algorithms.

N-terminal (Edman) sequencing

Samples of intact N-MADD-4B or its processing products, either in the liquid state or transferred from SDS-PAGE gels to PVDF membranes, were subjected to N-terminal sequencing by automated Edman degradation. For liquid samples, 500 pmol of protein were diluted to 100 μ l in TFA 0.1% (v/v), pH 2.0, and loaded on a ProSorb membrane pre-treated with 10 μ l methanol. The membrane was washed with TFA 0.1% (3 x 100 μ l) to fix and desalt the protein sample, and then loaded on a Shimadzu PPSQ 31B sequencer. Samples on PVDF membranes were stained with Ponceau red, then the membrane was washed three times with ethanol 90%, dried and loaded on the sequencer as above described. Seven to ten cycles were performed. N-MADD-4B was found to be preceded by an extra Asp residue arising from the cloning procedure (see **Supp. Fig. S1**).

Mass spectrometry (MS)

Protein identity in the SDS-PAGE bands was confirmed by peptide mass fingerprinting using Orbitrap LC-MS/MS while the monoisotopic masses of intact N-MADD-4 and its processing fragments were determined by MALDI-TOF-TOF MS, as described in the Supporting Information.

Microscale thermophoresis (MST)

Recombinant NLG-1, N-MADD-4B and TSP1-4 proteins were fluorescently labelled on Lys residues using Alexa647 fluor (Thermo-Fischer) and NHS ester conjugation according to the manufacturer's instructions. Briefly, the protein at 20 μ M was incubated with a 2-3-fold molar excess of dye (1 h, room temperature) and then loaded on a desalting column (NAP-5, GE Healthcare) to remove excess dye. Labelling efficiency was assessed by a protein-to-dye molar ratio of ca. 2:1, as measured at 280 nm and 650 nm, respectively. Differently, the Ig-like domain at 10 μ M was labelled on the N-terminal 6xHis tag using the Monolith His-Tag labelling kit RED-tris-NTA 2nd generation (NanoTemper Technologies) and the manufacturer's instructions (5 μ M, 1 h incubation at room temperature), given for labelling half of the protein population.

Labelled NLG-1 at 35 nM was incubated with unlabelled N-MADD-4B or N-MADD-4B _{Δ Ig} in the 73 nM to 12.5 μ M concentration range or with unlabelled TSP1-4 in the broader 0.8 nM to 25 μ M range, in the absence or presence of 250 μ M heparin sodium (Euromedex) or HPLC-purified decameric heparin or HS (a gift from Hugues Lortat-Jacob, IBS, Grenoble) (1.5 h, room temperature). Samples were briefly centrifuged and loaded into standard-treated capillaries (NanoTemper Technologies). Measurements were performed at 24°C in Hepes 20

mM, pH 7.5, NaCl 200 mM, supplemented with CaCl₂ 2 mM, Tween-20 0.1% (v/v) and BSA 0.2% (w/v), using the Monolith NT.115 apparatus (NanoTemper Technologies) with 40% led power and 80% IR-laser power. At least three independent experiments were performed, while each series of capillaries was read twice at 20 min interval. To record the Ig-like interaction with NLG-1 with optimal thermophoretic signal amplitude, we labelled the smaller Ig-like protein and incubated it at 150 nM with unlabelled NLG-1 in the 4.5 nM to 149 μM concentration range. Here, premium capillaries, 95% led power and 40% IR-laser power were used for data recording. Competition experiments were performed using a mix of labelled NLG-1 (35 nM) and unlabelled N-MADD-4B (1.25 μM) along with either unlabelled NLG-1 (7.6 nM to 125 μM) or heparin (4.6 nM to 150 μM) as a competitor, and the same experimental conditions as for the N-MADD-4B interaction with NLG-1.

MST data were analysed with the NanoTemper MO.Affinity Analysis software v2.2.4. Binding and competition curves were fitted to the data points using either the Law of mass action (Kd model, with calculation of the equilibrium dissociation constant, Kd) or the Hill model (calculation of the half-maximal effective concentration, EC₅₀) and the equations provided by the analysis software (see Supporting information).

Homology 3D modelling of the TSP1-4 and Ig-like domains

Homologues of N-MADD-4B with available 3D structures were identified from sequence processing by the HHpred server (60). Structures 1W0R and 1XIW were identified as suitable homologues (rank 1) for the TSP1-4 and Ig-like parts of N-MADD-4B, respectively, and used as molecular templates for homology modelling with MODELLER (61) using default parameters. Fig. 1C was generated with PyMol (The PyMol Molecular Graphics System, version 2.2.3, Schrödinger, LLC).

Data availability – The raw mass spectrometry data associated to Supp. Fig. S1 have been deposited to the ProteomeXchange Consortium via the PRIDE partner repository (<https://www.ebi.ac.uk/pride/>) with dataset identifier PXD020639.

Acknowledgements - This project was supported by the French ANR-15-CE11-0016 grant (to JLB and PM); the Campus France PRESTIGE-2017-1-0027 co-financing grant (to SP); the European Research Council ERC_Adg C.NAPSE #695295 grant (to JLB); and the French Infrastructure for Integrated Structural Biology (FRISBI) through ANR-10-INBS-05 grant. The Marseille Proteomics facility (marseille-proteomique.univ-amu.fr) is supported by ‘Infrastructures Biologie Santé et Agronomie’ (IBiSA); ‘Plateformes Technologiques Aix-Marseille’; ‘Cancéropôle PACA’; ‘Région Sud Provence-Alpes-Côte d'Azur’; ‘Institut Paoli-Calmettes’; ‘Centre de Recherche en Cancérologie de Marseille’ (CRCM); ‘Fonds Européen de Développement Régional’ (FEDER); and ‘Plan Cancer’. We thank Hugues Lortat-Jacob (Institut de Biologie Structurale, Grenoble, France) for the kind gift of purified heparin and HS samples, and

Plasmids and germline transformation

The control strain used in this study was EN296 *unc-49(kr296::tagRFP)* (62). Plasmids were pXZ066 [*Punc-47::madd-4(TSP1-4)-GFP*], pXZ067 [*Punc-47::madd-4(TSP1-4+Ig)-GFP*] and pXZ111 [*pmyo-3::madd-4(Ig)-GFP*]. Transgenes were created by conventional microinjection of plasmids at 15 ng/μl in the gonad of EN3218 *madd-4(kr270); unc-49(kr296::tagRFP)* animals, and named *krEx1319* and *krEx1320* for [*Punc-47::madd-4(TSP1-4)-GFP*] and *krEx1345* for [*pmyo-3::madd-4(Ig)-GFP*]. A single copy insertion allele was created using the miniMos technique for pXZ067 *krSi93[miniMos_Punc-47::madd-4(TSP1-4+Ig)-GFP]* (63).

Spinning disk microscopy imaging and quantification

Young adult hermaphrodites (24h post L4 larva stage) were used for imaging. Live worms were mounted on 2% agarose dry pads with 1% polylysine beads in M9 buffer. Fluorescence images were captured using an Andor spinning disk system installed on a Nikon-IX86 microscope (Olympus, Japan) equipped with a 60/1.2 oil immersion objective and an Evolve EMCCD camera. Each animal was imaged as a stack of optical sections (0.2 μm apart) containing 30-39 slices and projected along the Z-axis. Images were quantified using ImageJ (v1.48 by NIH) with Fiji plugin add-ons. Synaptic GABA_ARs were quantified as described previously (22, 64). Acquisition settings were the same for each experimental group. For fluorescence intensity measurement, 30 μm (wide) x 5 μm (high) regions along ventral (between VD6 and VD7 neuron) or dorsal cord near the anterior mid-body were cropped and analysed. For the MADD-4B(TSP1-4)-GFP rescue group, two independent extra-chromosome arrays were quantified, and the values were pooled together.

Maria Mate (Biophysical techniques facility, AFMB Lab, Marseille, France) for SEC-MALS. SP was a laureate of the Marie Skłodowska-Curie Actions Seal of Excellence Award on this project in 2017.

Author contributions - SP, BPL, JLB and PMarchot designed the research; SP produced, purified, characterised the recombinant proteins, performed the MST experiments, generated the structural models; XZ performed the *in vivo* experiments; VD created stable cell lines for production of recombinant NLG-1 and N-MADD-4B; BPL and HT generated the plasmidic constructs; PMansuelle performed N-terminal sequencing; PF performed mass spectrometry analyses; YB generated initial 3D models and defined construct boundaries; SP, BPL, PMansuelle, PF, JLB and PMarchot analysed the data; SP and PMarchot wrote the manuscript with contribution from all authors. All authors agreed on this version of the manuscript.

Conflict of interest: The authors declare that they have no conflicts of interest with the contents of this article.

References

- Biederer, T., and Massimiliano, S. (2008) Signalling by synaptogenic molecules. *Curr. Opin. Neurobiol.* **18**, 261-269.
- Yuzaki, M. (2018) Two classes of secreted synaptic organizers in the central nervous system. *Annu. Rev. Phys.* **80**, 243-262.
- Graf, E. R., Zhang, X., Jin, S-X., Linhoff, M. W., and Craig, A. M. (2004) Neurexins induce differentiation of GABA and glutamate postsynaptic specializations via neuroligins. *Cell* **119**, 1013-1026.
- Levinson, J. N., Chéry, N., Huang, K., Wong, T. P., Gerrow, K., Kang, R., Prange, O., Wang, Y. T., and El-Husseini E. (2005) Neuroligins mediate excitatory and inhibitory synapse formation: involvement of PSD-95 and neurexin-1 in neuroligin-induced synaptic specificity. *J. Biol. Chem.* **280**, 17312-17319.
- Chubykin, A. A., Atasoy, D., Etherton, M. R., Brose, N., Kavalali, E. T., Gibson, J. R., and Südhof, T. C. (2007) Activity-dependent validation of excitatory vs. inhibitory synapses by Neuroligin-1 vs. Neuroligin-2. *Neuron* **54**, 919-931.
- Scheiffele, P., Fan, J., Choih, J., Fetter, R., and Serafini, T. (2000) Neuroligin expressed in non-neuronal cells triggers presynaptic development in contacting axons. *Cell* **101**, 657-669.
- Fu, Z., Washbourne, P., Ortinski, P., and Vicini, S. (2003) Functional excitatory synapses in HEK293 cells expressing neuroligin and glutamate receptors. *J. Neurophysiol.* **90**, 3950-3957.
- Ko, J., Zhang, C., Arac, D., Boucard, A. A., Brunger, A. T., and Südhof, T. C. (2009) Neuroligin-1 performs neurexin-dependent and neurexin-independent functions in synapse validation. *EMBO J.* **28**, 3244-3255.
- Xu, J., Xiao, N., and Xia, J. (2010) Thrombospondin 1 accelerates synaptogenesis in hippocampal neurons through neuroligin 1. *Nat. Neurosci.* **13**, 22-24.
- Singh, S. K., Stogsdill, J. A., Pulimood, N. S., Dingsdale, H., Kim, Y. H., Pilaz, L. J., Kim, I. H., Manhaes, A. C., Rodrigues, W. S. Jr., Pamukcu, A., Enustun, E., Ertuz, Z., Scheiffele, P., Soderling, S. H., Silver, D. L., Ji, R. R., Medina, A. E., and Eroglu, C. (2016) Astrocytes assemble thalamocortical synapses by bridging NRX1a and NL1 via hevin. *Cell* **164**, 183-196.
- Elegheert, J., Cvetkovska, V., Clayton, A. J., Heroven, C., Vennekens, K. M., Smukowski, S. N., Regan, M. C., Jia, W., Smith, A. C., Furukawa, H., Savas, J. N., de Wit, J., Begbie, J., Craig, A-M., and Aricescu, A. R. (2017) Structural mechanism for modulation of synaptic neuroligin-neurexin signalling by MDGA Proteins. *Neuron* **95**, 896-913.
- Ting, J. T., Peça, J., and Feng, G. (2012) Functional consequences of mutations in postsynaptic scaffolding proteins and relevance to psychiatric disorders. *Annu. Rev. Neurosci.* **35**, 49-71.
- Selkoe, D. J. (2002) Alzheimer's disease is a synaptic failure. *Science* **298**, 789-791.
- Südhof, T. C. (2008) Neuroligins and neurexins link synaptic function to cognitive disease. *Nature* **455**, 903-911.
- Connor, S. A., Ammendrup-Johnsen, I., Chan, A. W., Kishimoto, Y., Murayama, C., Kurihara, N., Tada, A., Ge, Y., Lu, H., Yan, R., LeDue, J. M., Matsumoto, H., Kiyonari, H., Kirino, Y., Matsuzaki, F., Suzuki, T., Murphy, T. H., Wang, Y. T., Yamamoto, T., and Craig, A-M. (2016) Altered cortical dynamics and cognitive function upon haploinsufficiency of the autism-linked excitatory synaptic suppressor MDGA2. *Neuron* **91**, 1052-1068.
- Kähler, A. K., Djurovic, S., Kulle, B., Jönsson, E. G., Agartz, I., Hall, H., Opjordsmoen, S., Jakobsen, K.

- D., Hansen, T., Melle, I., Werge, T., Steen, V. M., and Andreassen, O. A. (2008) Association analysis of schizophrenia on 18 genes involved in neuronal migration: MDGA1 as a new susceptibility gene. *Am. J. Med. Genet. B Neuropsychiatr. Genet.* **147B**, 1089-1100.
17. Li, J., Liu, J., Feng, G., Li, T., Zhao, Q., Li, Y., Hu, Z., Zheng, L., Zeng, Z., He, L., Wang, T., and Shi, Y. (2011) The MDGA1 gene confers risk to schizophrenia and bipolar disorder. *Schizophr. Res.* **125**, 194-200.
 18. Zhou, X., and Bessereau, J-L. (2019) Molecular architecture of genetically-tractable GABA synapses in *C. elegans*. *Front. Mol. Neurosci.* **12**, 304 (Review).
 19. Pinan-Lucarré, B., Tu, H., Pierron, M., Ibáñez Cruceyra, P., Zhan, H., Stigloher, C., Richmond, J. E., and Bessereau, J-L. (2014) *C. elegans* Punctin specifies cholinergic versus GABAergic identity of postsynaptic domains. *Nature* **511**, 466-470.
 20. Hunter, J. W., Mullen, G. P., McManus, J. R., Heatherly, J. M., Duke, A., and Rand, J. B. (2010) Neuroigin-deficient mutants of *C. elegans* have sensory processing deficits and are hypersensitive to oxidative stress and mercury toxicity. *Dis. Model. Mech.* **3**, 366-376.
 21. Hu, Z., Hom, S., Kudze, T., Tong, X-J., Choi, S., Aramuni, G., Zhang, W., and Kaplan, J. M. (2012) Neurexin and neuroigin mediate retrograde synaptic inhibition in *C. elegans*. *Science* **337**, 980-984.
 22. Tu, H., Pinan-Lucarré, B., Ji, T., Jospin, M., and Bessereau, J-L. (2015) *C. elegans* punctin clusters GABAA receptors via neuroigin binding and UNC-40/DCC recruitment. *Neuron* **86**, 1407-1419.
 23. Maro, G. S., Gao, S., Olechwier, A. M., Hung, W. L., Liu, M., Özkan, E., Zhen, M., and Shen, K. (2015) MADD-4/Punctin and neurexin organize *C. elegans* GABAergic postsynapses through neuroigin. *Neuron* **86**, 1420-1432.
 24. Hubmacher, D., and Apte, S. S. (2015) ADAMTS proteins as modulators of microfibril formation and function. *Matrix Biol.* **47**, 34-43.
 25. Ferrer-Ferrer, M., and Dityatev, A. (2018) Shaping synapses by the neural extracellular matrix. *Front. Neuroanat.* **12**, 40-56.
 26. Krishnaswamy, V. R., Benbenishty, A., Blinder, P., and Sagi, I. (2019) Demystifying the extracellular matrix and its proteolytic remodeling in the brain: structural and functional insights. *Cell. Mol. Life Sci.* **76**, 3229-3248.
 27. Dow, D. J., Huxley-Jones, J., Hall, J. M., Francks, C., Maycox, P. R., Kew, J. N. C., Gloger, I. S., Mehta, N. A. L., Kelly, F. M., Muglia, P., Breen, G., Jugurnauth, S., Pederoso, I., St.Clair, D., Rujescu, D., and Barnes, M. R. (2011) ADAMTSL3 as a candidate gene for schizophrenia: Gene sequencing and ultra-high density association analysis by imputation. *Schizophr. Res.* **127**, 28-34.
 28. Hamel, M. G., Ajmo, J. M., Leonardo, C. C., Zuo, F., Sandy, J. D., and Gottschall, P. E. (2008) Multimodal signaling by the ADAMTSs (a disintegrin and metalloproteinase with thrombospondin motifs) promotes neurite extension. *Exp. Neurol.* **210**, 428-440.
 29. Chelini, G., Pantazopoulos, H., Durning, P., and Berretta, S. (2018) The tetrapartite synapse: a key concept in the pathophysiology of schizophrenia. *Eur. Psychiatry* **50**, 60-69.
 30. Pantazopoulos, H., Woo, T-U. W., Lim, M. P., Lange, N., and Berretta, S. (2010) Extracellular matrix-glia abnormalities in the amygdala and entorhinal cortex of subjects diagnosed with schizophrenia. *Arch. Gen. Psychiatry.* **67**, 155-166.
 31. Gendron, C., Kashiwagi, M., Lim, N. H., Enghild, J. J., Thøgersen, I. B., Hughes, C., Caterso, B., and Nagase, H. (2007) Proteolytic activities of human ADAMTS-5 comparative studies with ADAMTS-4. *J. Biol. Chem.* **282**, 18294-18306.
 32. Tsutsui, K., Manabe, R., Yamada, T., Nakano, I., Oguri, Y., Keene, D. R., Sengle, G., Sakai, L. Y., and Sekiguchi, K. (2010) ADAMTSL-6 is a novel extracellular matrix protein that binds to fibrillin-1 and promotes fibrillin-1 fibril formation. *J. Biol. Chem.* **285**, 4870-4882.
 33. Bader, H. L., Wang, L. W., Ho, J. C., Tran, T., Holden, P., Fitzgerald, J., Atit, R. P., Reinhardt, D. P., and Apte, S. S. (2012) A disintegrin-like and metalloprotease domain containing thrombospondin type 1 motif-like 5 (ADAMTSL5) is a novel fibrillin-1-, fibrillin-2-, and heparin-binding member of the ADAMTS superfamily containing a netrin-like module. *Matrix Biol.* **31**, 398-411.
 34. Colige, A., Ruggiero, F., Vandenbergh, I., Dubail, J., Kesteloot, F., Van Beeumen, J., Beschin, A., Brys, L., Lapière, C. M., and Nusgens, B. (2005) Domains and maturation processes that regulate the activity of ADAMTS-2, a metalloproteinase cleaving the aminopropeptide of fibrillar procollagens types I-III and V. *J. Biol. Chem.* **280**, 34397-34408.
 35. Rao, N., Ke, Z., Liu, H., Ho, C-J., Kumar, S., Xiang, W., Zhu, Y., and Ge, R. (2013) ADAMTS4 and its

- proteolytic fragments differentially affect melanoma growth and angiogenesis in mice. *Int. J. Cancer* **133**, 294-307.
36. Hubmacher, D., Wang, L. W., Mecham, R. P., Reinhardt, D. P., and Apte S. S. (2015) Adamts12 deletion results in bronchial fibrillin microfibril accumulation and bronchial epithelial dysplasia – a novel mouse model providing insights into geophytic dysplasia. *Disease Model Mech.* **8**, 487-499.
 37. Seetharaman, A., Selman, G., Puckrin, R., Barbier, L., Wong, E., D'Souza, S. A., and Roy, P. J. (2011) MADD-4 is a secreted cue required for midline-oriented guidance in *Caenorhabditis elegans*. *Dev. Cell* **21**, 669-680.
 38. Vasudevan, D., and Haltiwanger, R. S. (2014) Novel roles for O-linked glycans in protein folding. *Glycoconj. J.* **31**, 417-426.
 39. Kozma, K., Keusch, J. J., Hegemann, B., Luther, K. B., Klein, D., Hess, D., Haltiwanger, R. S., and Hofsteenge, J. (2006) Identification and characterization of a β 1,3-Glucosyltransferase that synthesizes the Glc- β 1,3-Fuc disaccharide on thrombospondin type 1 repeats. *J. Biol. Chem.* **281**, 36742-36751.
 40. Flatmark, T., and Sletten, K. (1968) Multiple forms of cytochrome c oxidase in the rat. *J. Biol. Chem.* **243**, 1623-1629.
 41. Midelfort, C. F., and Mehler, A. H. (1972) Deamidation in vivo of an asparagine residue of rabbit muscle aldolase. *Proc. Natl. Acad. Sci. U. S. A.* **69**, 1816-1819.
 42. Robinson, N. E., and Robinson, A. B. (2001) Molecular clocks. *Proc. Natl. Acad. Sci. U. S. A.* **98**, 944-949.
 43. Stephenson, R. C., and Clarke, S. (1989) Succinimide formation from aspartyl and asparaginyl peptides as a model for the spontaneous degradation of proteins. *J. Biol. Chem.* **264**, 6164-6170.
 44. Deverman, B. E., Cook, B. L., Manson, S. R., Niederhoff, R. A., Langer, E. M., Rosova, I., Kulans, L. A., Fu, X., Weinberg, J. S., Heinecke, J. W., Roth, K. A., and Weintraub, S. J. (2002) Bcl-xL deamidation is a critical switch in the regulation of the response to DNA damage. *Cell* **111**, 51-62.
 45. Curnis, F., Longhi, R., Crippa, L., Cattaneo, A., Dondossola, E., Bachi, A., and Corti, A. (2006) Spontaneous formation of L-isoaspartate and gain of function in fibronectin. *J. Biol. Chem.* **281**, 36466-36476.
 46. Wilkinson, K. D. (2004) Quantitative analysis of protein-protein interactions. *Methods Mol. Biol.* **261**, 15-32.
 47. Gao, G., Westling, J., Thompson, V. P., Howell, T. D., Gottschall, P. E., and Sandy, J. D. (2002) Activation of the proteolytic activity of ADAMTS4 (Aggrecanase-1) by C-terminal truncation. *J. Biol. Chem.* **277**, 11034-11041.
 48. Kashiwagi, M., Enghild, J. J., Gendron, C., Hughes, C., Caterson, B., Itoh, Y., and Nagase, H. (2004) Altered proteolytic activities of ADAMTS-4 expressed by C-terminal processing. *J. Biol. Chem.* **279**, 10109-10119.
 49. Kim, J. A., Kim, D., Won, S. Y., Han, K. A., Park, D., Cho, E., Yun, N., An, H. J., Um, J. W., Kim, E., Lee, J. O., Ko, J., and Kim, H. M. (2017) Structural insights into modulation of neuroligin-neurexin trans-synaptic adhesion by MDGA1/neuroligin-2 complex. *Neuron* **94**, 1121-1131.
 50. Gangwar, S. P., Zhong, X., Seshadrinathan, S., Chen, H., Machius, M., and Rudenko, G. (2017) Molecular mechanism of MDGA1: regulation of neuroligin 2: neuroligin trans-synaptic bridges. *Neuron* **94**, 1132-1141.
 51. Miller, M. T., Mileni, M., Comoletti, D., Stevens, R. C., Harel, M., and Taylor, P. (2011) The crystal structure of the α -neuroligin-1 extracellular region reveals a hinge point for mediating synaptic adhesion and function. *Structure* **19**, 767-78.
 52. Chen, F., Venugopal, V., Murray, B., and Rudenko, G. (2011) The structure of neuroligin 1 α reveals features promoting a role as synaptic organizer. *Structure* **19**, 779-789.
 53. Zhang, P., Lu, H., Peixoto, R. T., Pines, M. K., Ge, Y., Oku, S., Siddiqui, T. J., Xie, Y., Wu, W., Archer-Hartmann, S., Yoshida, K., Tanaka, K. F., Aricescu, A. R., Azadi, P., Gordon, M. D., Sabatini, B. L., Wong, R. O. L., and Craig A-M. (2018) Heparan sulfate organizes neuronal synapses through neuroligin partnerships. *Cell* **174**, 1-15.
 54. Whalen, D. M., Malinauskas, T., Gilbert, R. J. C., and Siebold C. (2013) Structural insights into proteoglycan-shaped Hedgehog signalling. *Proc. Natl. Acad. Sci. U. S. A.* **110**, 16420-16425.
 55. Ai, X., Do, A-T., Lozynska, O., Kusche-Gullberg, M., Lindahl U., and Emerson C. P. Jr. (2003) QSulf1 remodels the 6-O sulfation states of cell surface heparan sulfate proteoglycans to promote Wnt signaling. *J. Cell Biol.* **162**, 341-351.

56. Flannery, C. R., Zeng, W., Corcoran, C., Collins-Racie, L. A., Chockalingam, P. S., Hebert, T., Mackie, S. A., McDonagh, T., Crawford, T. K., Tomkinson, K. N., LaVallie, E. R., and Morris, E. A. (2002) Autocatalytic cleavage of ADAMTS-4 (Aggrecanase-1) reveals multiple glycosaminoglycan-binding sites. *J. Biol. Chem.* **277**, 42775-42780.
57. Colige, A. C. (2020) Challenges and solutions for purification of ADAMTS proteases: an overview. *Methods Mol. Biol.* **2043**, 45-53.
58. Kramerova, I. A., Kawaguchi, N., Fessler, L. I., Nelson, R. E., Chen, Y., Kramerova, A., Kusche-Gullberg, M., Kramer, J. M., Ackley, B. D., Sieron, A. L., Prockop, D. J., and Fessler, J. (2000) Papilin in development; a pericellular protein with a homology to the ADAMTS metalloproteinases. *Development* **127**, 5475-5485.
59. Tom, R., Bisson, L., and Durocher, Y. (2008) Culture of HEK293-EBNA1 cells for production of recombinant proteins. *Cold Spring Harb. Protoc.* **3**, 1-5.
60. Zimmermann, L., Stephens, A., Nam, S-Z., Rau, D., Kübler, J., Lozajic, M., Gabler, F., Söding, J., Lupas, A. N., and Alva, V. (2018) A completely re-implemented MPI bioinformatics toolkit with a new HHpred server at its core. *J. Mol. Biol.* **430**, 2237-2243.
61. Sanchez, R., and Sali, A. (1997) Evaluation of comparative protein structure modelling by MODELLER-3. *Proteins* **1**, 50-58.
62. Zhou, X., Gueydan, M., Jospin, M., Ji, T., Valfort, A., Pinan-Lucarré, B., Bessereau, J-L. (2020). The netrin receptor UNC-40/DCC assembles a postsynaptic scaffold and sets the synaptic content of GABA_A receptors. *Nat. commun.* **11**, 2674.
63. Frøkjær-Jensen, C., Davis, M. W., Sarov, M., Saroy, M., Taylor, J., Flibotte, S., LaBella, M., Pozniakivsky, A., Moerman, D. G., and Jorgensen, E. M. (2014) Random and targeted transgene insertion in *Caenorhabditis elegans* using a modified Mos1 transposon. *Nat. Methods* **11**, 529-534.
64. Boulin, T., Rapti, G., Briseño-Roa, L., Stigloher, C., Richmond, J. E., Paoletti, P., and Bessereau, J-L. (2012) Positive modulation of a Cys-loop acetylcholine receptor by an auxiliary transmembrane subunit. *Nat. Neurosci.* **15**, 1374-1381.

Table 1. N-terminal sequences detected by Edman degradation from liquid N-MADD-4B samples. Samples ‘N-MADD-4B’ and ‘N-MADD-4B fragments’ correspond to lanes 1 and 2, respectively, of the SDS-PAGE gel displayed in Fig. 3A. Abundance values (rounded-up) are indicated.

N-MADD-4B		N-MADD-4B fragments	
D ¹ NHNDWQAP ⁹	90%	D ¹ NHNDWQAP ⁹	90%
		S ⁷⁸ EDEAPYQWR ⁸⁷	10%
R ²⁷⁵ VFEQNAEQK ²⁸⁴	5%	R ²⁷⁵ VFEQNAEQK ²⁸⁴	1%
S ²⁷³ NRVFEQNAE ²⁸²	3%	S ²⁷³ NRVFEQNAE ²⁸²	1%
E ²⁸² QKKLTLGIG ²⁹¹	2%	E ²⁸² QKKLTLGIG ²⁹¹	2.5%
T ¹⁷⁵ DGADAHIVL ¹⁸⁴	2%	T ¹⁷⁵ DGADAHIVL ¹⁸⁴	0.5%

Table 2. Fit parameters obtained for MST experiments between N-MADD-4B and labelled NLG-1 (NLG*) or NLG-1 and labelled Ig (Ig*). The N-MADD-4B/ NLG* binding data (Fig. 4A), N-MADD-4B/ NLG*/ NLG-1 competition data (Fig. 4B) and NLG-1/ Ig* binding data (Fig. 4C) were processed using either the Kd or the Hill model (see Experimental procedures).

Fit parameters	Kd model	Hill model
N-MADD-4B/ NLG*		
Kd or EC50 (nM)	465	578
Kd confidence (nM)	± 130	± 77
Standard error (nM)	1.3	1.2
Reduced χ^2	1.6	0.8
Signal / noise	14.9	13.1
Hill coefficient	-	2.3
N-MADD-4B/ NLG*/ NLG-1		
Kd or EC50 (nM)	1428	1396
Kd confidence (nM)	± 488	± 285
Standard error (nM)	0.8	0.8
Reduced χ^2	1.1	1.1
Signal / noise	17.8	17.5
Hill coefficient	-	1.0
NLG-1/ Ig*		
Kd or EC50 (nM)	6139	5580
Kd confidence (nM)	± 1220	± 825
Standard error (nM)	1.4	1.3
Reduced χ^2	0.5	0.2
Signal / noise	16.1	16.3
Hill coefficient	-	1.4

Table 3. Fit parameters obtained for N-MADD-4B binding to labelled NLG-1 (NLG*) in the presence or absence of heparin. The N-MADD-4B/ NLG* binding data from experiments performed in absence or presence of heparin (Fig. 5A) and the N-MADD-4B/ NLG*/ heparin competition data (Fig. 5B) were processed using the Hill model (see Experimental procedures).

Fit parameters	Binding - heparin	Binding + heparin	Competition experiment
Kd or EC50 (nM)	467	1782	740
Kd confidence (nM)	± 31	± 483	± 136
Standard error (nM)	0,9	0,8	1.0
Reduced χ^2	0.6	1.0	6.9
Signal to noise	14.5	17.1	6.7
Hill coefficient	4.3	1.1	3.0

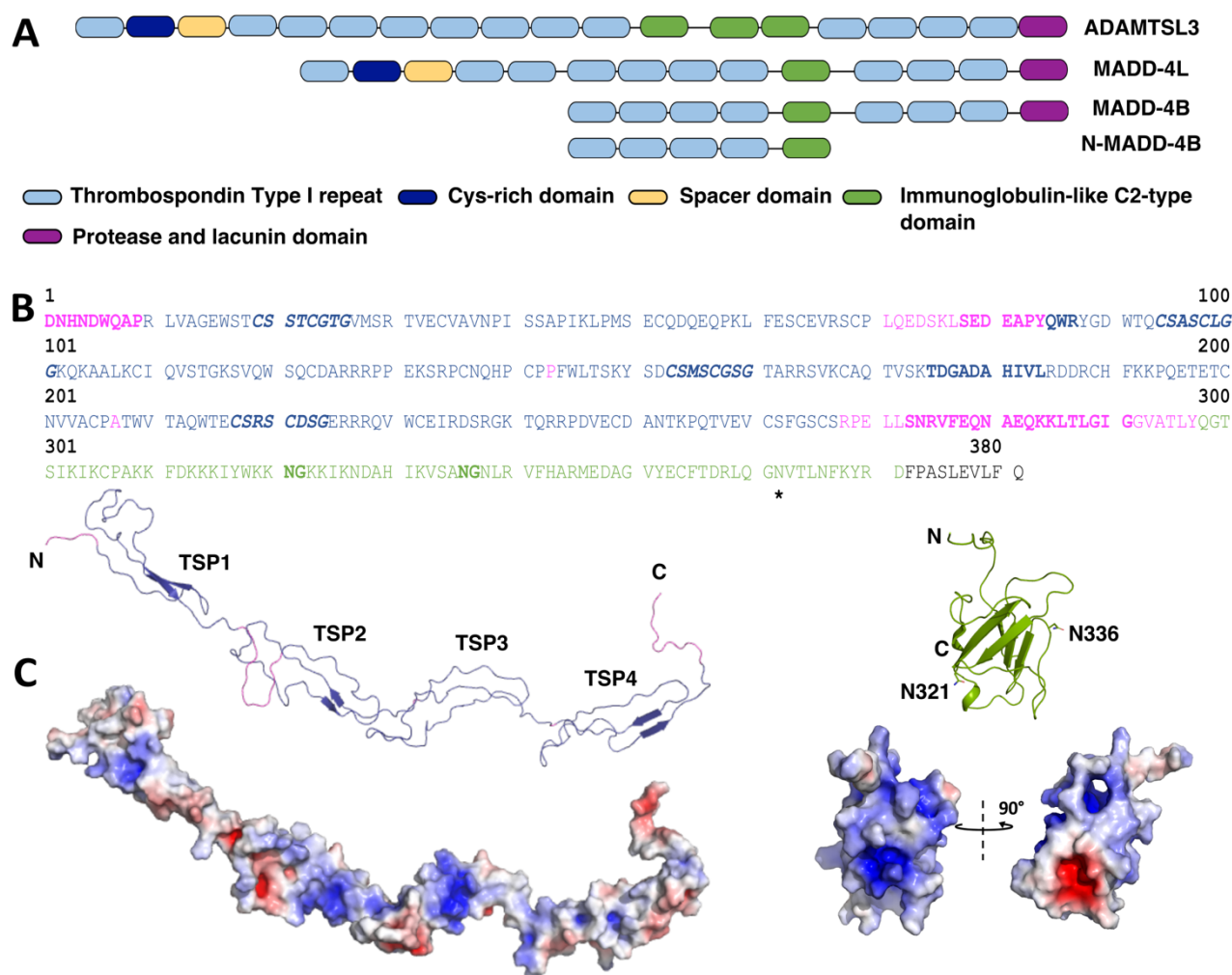


Figure 1. N-MADD-4B domain organisation, sequence and structural model. *A*, Domain organisation of human ADAMTSL3, *C. elegans* MADD-4L and MADD-4B and the recombinant N-MADD-4B in their secreted form. *B*, Sequence of N-MADD-4B with the TSP1-4 domains coloured in blue, linker regions in magenta and the Ig-like domain in green. CXX(S/T)CXXG consensus motifs for O-fucosylation are displayed in bold blue italics and the potentially N-glycosylated Asn362 is indicated by a star. The sequences identified by Edman degradation are in bold. The two sites for potential deamidation (N³²¹G, N³³⁶G) in the Ig-like domain are shown in bold green. The C-terminal LEVL**FQ** hexapeptide is a leftover from the 3C-Protease cleavage site of the expressed fusion protein. *C*, Structural models of the TSP1-4 and Ig-like domains generated by homology and displayed on scale. The ribbon representations use the same colour codes as in panel A. The molecular surface representations show the distribution of electrostatic potentials from -5 k_BT/e_c (red) to $+5$ k_BT/e_c (blue). Two orientations, identical to that of the ribbon model (left) and 90° apart (right), of the overall positively charged Ig-like domain (theoretical pI, 9.8) evidence two pockets, strongly positively and negatively charged, on opposite faces of the domain.

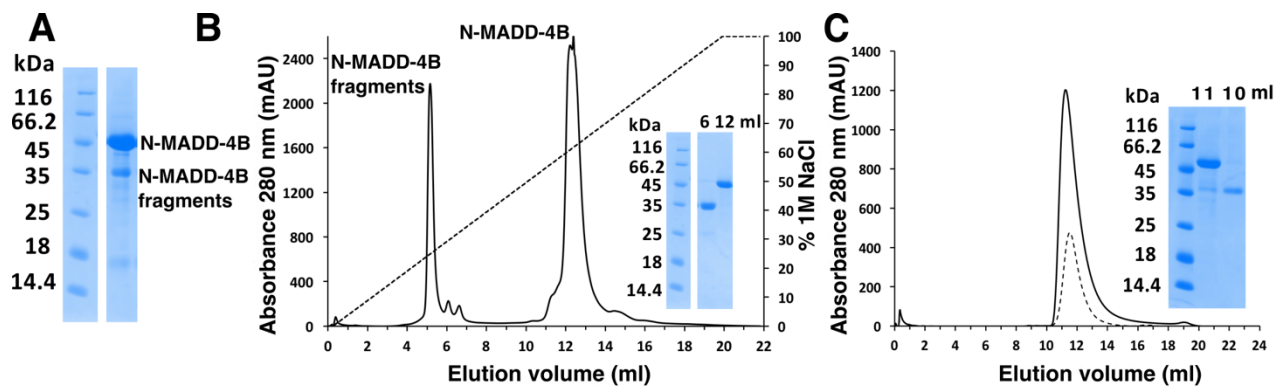


Figure 2. N-MADD-4B undergoes processing. *A*, SDS-PAGE analysis of peak elution fraction from affinity chromatography (Protein A, data not shown) evidenced intact N-MADD-4B (apparent mass, ca. 45 kDa) and N-MADD-4B fragments (≤ 35 kDa). The protein identity in each band was confirmed by mass spectrometry (see Supp. Fig. S1). *B*, Cation-exchange chromatography (MonoS, NaCl gradient) resolves the N-MADD-4B fragments (elution volume, 5-6 ml) from intact N-MADD-4B (12-13 ml). Inset: SDS-PAGE analysis of the peak elution fractions. *C*, Size-exclusion chromatography (Superdex-75 10/300) does not resolve intact N-MADD-4B (solid line) from the fragments (dashed line). Inset: SDS-PAGE analysis of the peak elution fractions.

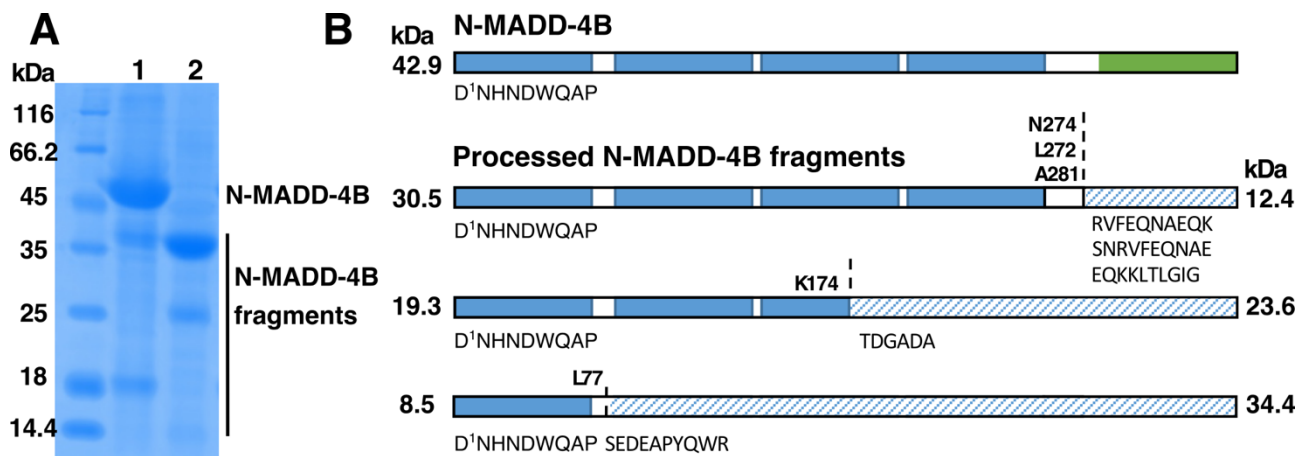


Figure 3. C-terminal processing of N-MADD-4B results eliminates the Ig-like domain. *A*, N-MADD-4B fragments are found as a minority in the freshly purified sample (lane 1) and as a majority in the processed sample (lane 2). The protein identity in each band was confirmed by mass spectrometry (see Supp. Fig. S1). *B*, Representation of the N-MADD-4B domains (blue TSP, green Ig-like) and the protein fragments identified by N-terminal sequencing (Table 1). The identified sequences account predominantly for the N-MADD-4B N-terminus (ca. 90% abundance) and marginally for its C-terminus (<10% abundance, shaded) denoting degradation within the C-terminal part of the protein. The theoretical mass of each detected fragment is indicated on either side of the scheme.

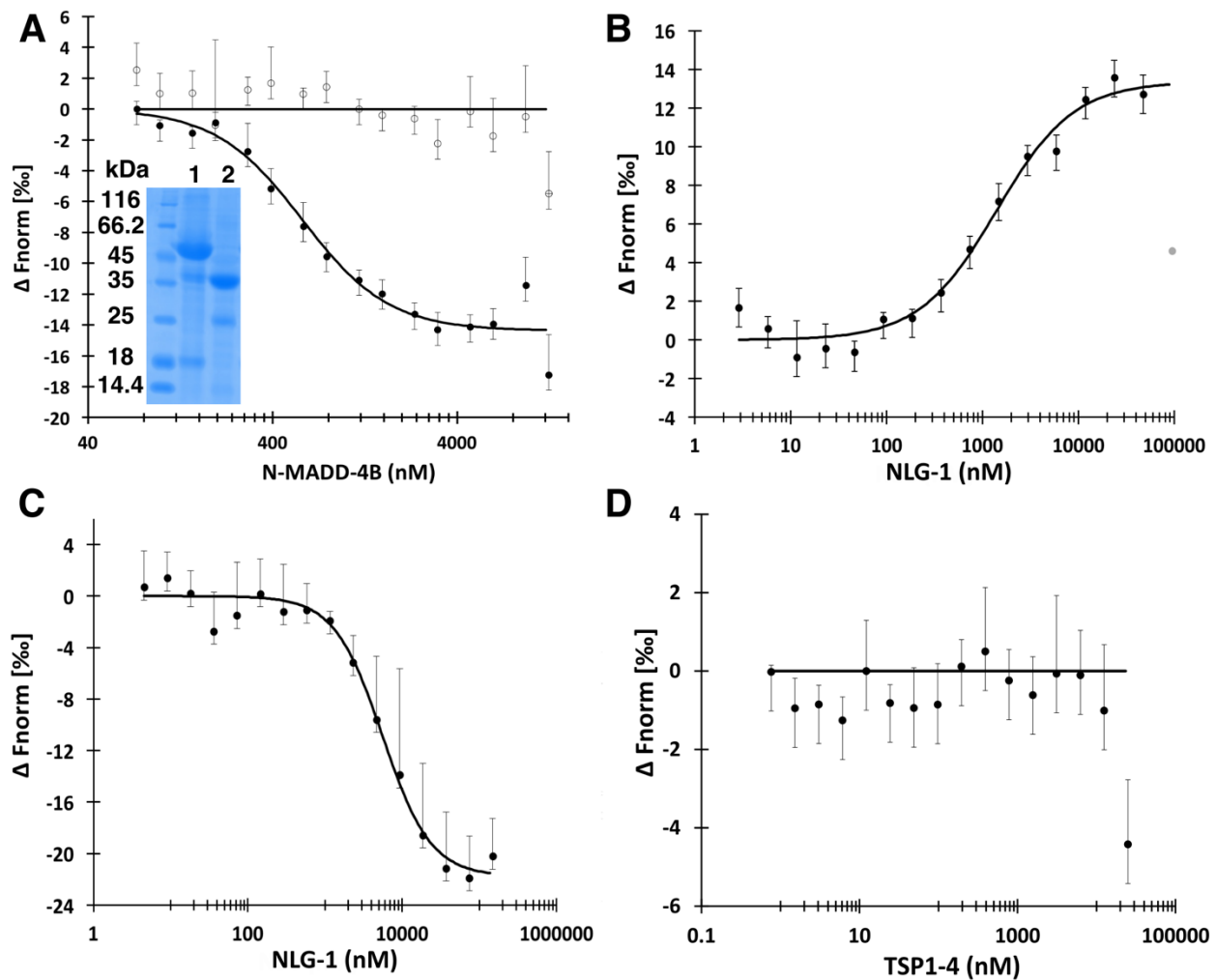


Figure 4. N-MADD-4B interacts with NLG-1 through the Ig-like domain. **A**, N-MADD-4B (73 nM to 12.5 μ M) comprising mostly the intact protein (see lane 1 of inserted SDS-PAGE (same gel as in Fig. 3A)) binds to labelled NLG-1 (35 nM) with an estimated K_d of 578 ± 77 nM (circles, $n = 4$) whereas N-MADD-4B $_{\Delta Ig}$ (lane 2 of inserted SDS-PAGE) does not bind (empty circles, $n = 3$). **B**, NLG-1 (38 nM to 125 μ M) competes with labelled NLG-1 (35 nM) for binding to N-MADD-4B (1.25 μ M) with an estimated K_d of 1396 ± 285 nM ($n = 3$). One outlier data point excluded from the fit is displayed in grey. **C**, NLG-1 (4.5 nM to 140 μ M) interacts with the labelled Ig-like domain (150 nM) with an estimated K_d of 5580 ± 825 nM ($n = 3$). **D**) TSP1-4 (3.5 nM to 25 μ M) does not interact with labelled NLG-1 (35 nM) ($n=3$). Error bars represent the standard deviation. All fit parameters are summarised in Table 2.

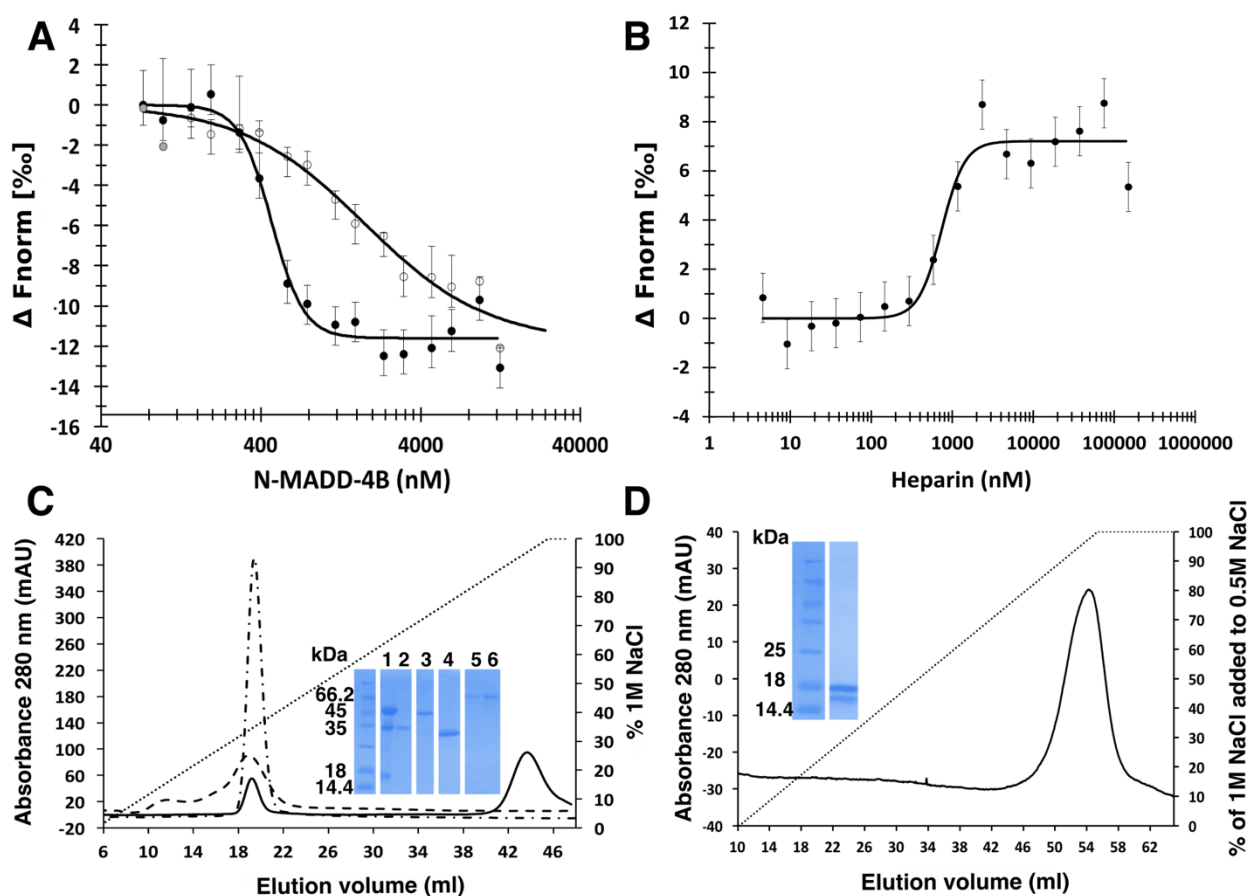


Figure 5. Heparin challenges the N-MADD-4B interaction with NLG-1. *A*, Binding of N-MADD-4B (73 nM to 12.5 μ M) to labelled NLG-1 (35 nM) (filled circles) is compromised in the presence of heparin (250 μ M) (empty circles). Three outlier data points excluded from the fit are displayed in grey. *B*, Heparin (4.5 nM to 150 μ M) prevents binding of N-MADD-4B (1 μ M) to labelled NLG-1 (35 nM) with a half-effect at ca. 740 nM. *C*, Relative affinities of N-MADD-4B fragments (solid line), TSP1-4 (dash-dotted line) and NLG-1 (dashed line) for immobilised heparin using NaCl elution (0 to 1M gradient over 8 CV) and conductivity recording. Inset: SDS-PAGE of N-MADD-4B input (lane 1) and of the the peak elution fractions of N-MADD-4B fragment (lane 2), intact MADD-4B (lane 3), TSP1-4 (lane 4); NLG-1 (lanes 5-6). Intact N-MADD-4B is retained much more strongly (elution at 82 mS/cm, i.e., 900 mM NaCl) than N-MADD-4B $_{\Delta Ig}$ (343 mM NaCl, i.e., 22.6 mS/cm), TSP1-4 (349 mM NaCl, i.e., 21.6 mS/cm) or NLG-1 (337 mM NaCl, i.e., 21.9 mS/cm). *D*, Relative affinity of the isolated Ig-like domain for immobilised heparin (0.5 M to 1.0 M NaCl gradient over 9 CV). The Ig-like domain is as strongly retained as intact N-MADD-4B. Inset: SDS-PAGE of the Ig-like elution fraction in which partial degradation is visible. (All proteins were loaded on the heparin column as 0.5 ml at 0.8 mg/ml.)

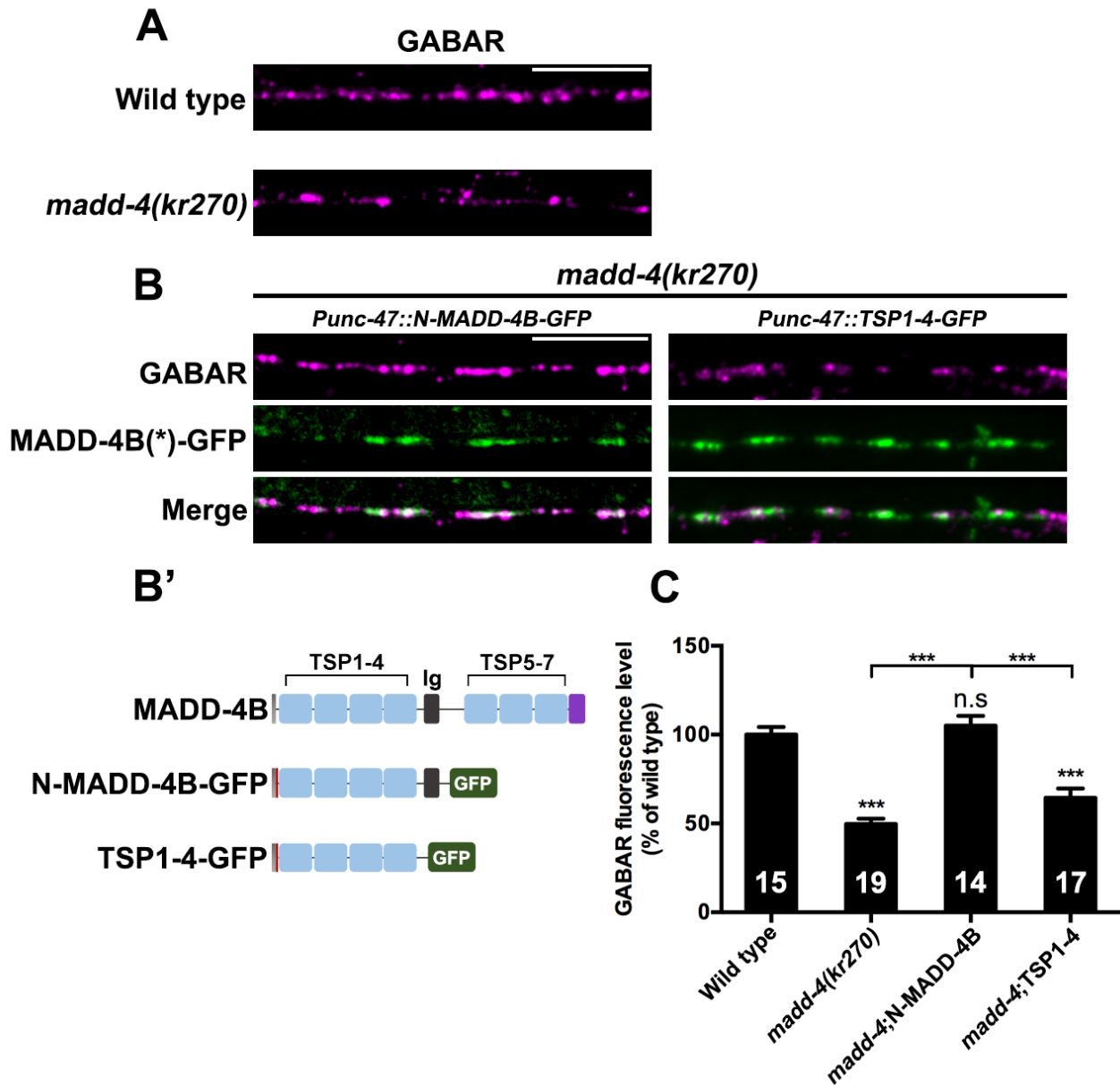


Figure 6. N-MADD-4B rescues GABA_AR clustering defect in the *C. elegans* MADD-4 null mutant. *A*, Confocal detection of RFP-GABA_AR expressed from the *unc-49::rfp* knock-in locus *kr296* in wild-type or *madd-4(kr270)* null mutant animals (magenta). *B*, N-MADD-4B-GFP or TSP1-4-GFP were expressed in GABAergic neurons of *madd-4(kr270)* mutant animals. The MADD-4B(*)-GFP row corresponds to N-MADD-4B-GFP (left panels) or TSP1-4-GFP (right panels). *B'*, Functional domains of MADD-4B, N-MADD-4B and TSP1-4. Grey: signal peptide; red: T7 tag; purple: PLAC domain. *C*, RFP-GABA_AR fluorescence levels were quantified in wild-type, *madd-4(kr270)*, N-MADD-4B and TSP1-4 rescue groups, and normalized to the wild type group (mean ± SEM). One-way ANOVA followed by Tukey's multiple comparisons test. *** $p < 0.001$. n.s, not significant. The numbers of animals are indicated inside the histogram boxes. Scale bar, 10 μm.

The Ig-like domain of Punctin/MADD-4 is the primary determinant for interaction with the ectodomain of neuroligin NLG-1

Semeli Platsaki, Xin Zhou, Bérangère Pinan-Lucarré, Vincent Delauzun, Haijun Tu, Pascal Mansuelle, Patrick Fourquet, Yves Bourne, Jean-Louis Bessereau and Pascale Marchot

J. Biol. Chem. published online September 14, 2020

Access the most updated version of this article at doi: [10.1074/jbc.RA120.014591](https://doi.org/10.1074/jbc.RA120.014591)

Alerts:

- [When this article is cited](#)
- [When a correction for this article is posted](#)

[Click here](#) to choose from all of JBC's e-mail alerts